A New Radio Frequency Interference Filter for Weather Radars

JOHN Y. N. CHO

Lincoln Laboratory, Massachusetts Institute of Technology, Lexington, Massachusetts

(Manuscript received 14 February 2017, in final form 4 April 2017)

ABSTRACT

A new radio frequency interference (RFI) filter algorithm for weather radars is proposed in the two-dimensional (2D) range-time/sample-time domain. Its operation in 2D space allows RFI detection at lower interference-to-noise or interference-to-signal ratios compared to filters working only in the sample-time domain while maintaining very low false alarm rates. Simulations and real weather radar data with RFI are used to perform algorithm comparisons. Results are consistent with theoretical considerations and show the 2D RFI filter to be a promising addition to the signal processing arsenal against interference with weather radars. Increased computational burden is the only drawback relative to filters currently used by operational systems.

1. Introduction

The radio frequency (RF) spectrum is a global resource that is under increasing demand by various parties. It is used for communications, remote sensing, navigation, etc., by public (military and civilian) and private sectors alike. Although there are national and international regulations and enforcement agencies that are meant to keep systems isolated from each other, the push to add more devices that utilize the RF spectrum has often resulted in unwanted interference. Of particular concern to the meteorology community is the significant uptick in RF interference (RFI) to weather radars from wireless telecommunication devices in the last decade (Saltikoff et al. 2016). RFI can prevent the retrieval of meteorological information by a weather radar in affected azimuthal sectors and present false data that might be mistaken for actual atmospheric observations. Ideally, regulations would be in place and effectively enforced such that RFI does not occur at all. However, as this is not the reality, we need to develop and implement the best possible means for mitigating the effects of RFI on weather radar data. This report documents an investigation of a potential new technique for RFI filtering.

Current weather radars have varying requirements and capabilities for RFI removal. For example, the Terminal Doppler Weather Radar (TDWR) specifications call for detection and flagging of asynchronous RF pulse interference (FAA 1995). This requirement is currently met by a single pulse anomaly detection filter applied to in-phase and quadrature (I&Q) time series data; the flagged pulses are replaced by interpolated values based on the adjacent pulses (Vaisala 2016). The Weather Surveillance Radar-1988 Doppler (WSR-88D), more commonly known as the Next Generation Weather Radar (NEXRAD), does not have a requirement for RFI detection and filtering, and none is currently implemented. It is, therefore, very susceptible to even low duty cycle pulsed interference.

As for federal regulations, the Radar Spectrum Engineering Criteria (RSEC), published by the National Telecommunications and Information Administration (NTIA), includes only a recommendation that radar systems operating in the 2700–2900-MHz band, of which NEXRAD is one type, should have provisions to suppress asynchronous pulsed interference (NTIA 2015). The range of conditions under which such suppression should be effective is [measured at the intermediate frequency (IF) receiver output] 1) peak interference-to-noise ratio (INR) < 50 dB, 2) pulse width of 0.5–4.0 μs, and 3) pulse repetition frequency (PRF) of 100–2000 Hz. Note that these conditions cover only low duty cycles ($\leq$0.8%) and that the RFI suppression by the receiver is only a recommendation, not a requirement.

Looking to the future, there will be ever more incentive to maximize the RF spectrum usage efficiency of devices and networks. While there are RF bands that are

Corresponding author: John Y. N. Cho, jync@ll.mit.edu

DOI: 10.1175/JTECH-D-17-0028.1

reserved for federal government operations, there is mounting pressure to release parts of these bands for commercial use. The monetary value of RF spectrum windows suitable for commercial exploitation is, indeed, sky high, and clearly more bandwidth made available to the public is desirable for economic growth. The government itself realizes this, as exemplified by the White House memorandum declaring that 500 MHz of the federally reserved spectrum be opened for sharing in 10 years (Obama 2010). But in order to realize such an ambitious goal without jeopardizing the services that existing systems render to critical missions, more functions will have to be squeezed into the same spectral space.

At the same time, there is a technological trend in radar design that runs counter to spectrum usage efficiency. Solid-state transmitters are becoming more popular for radar applications. Their primary advantage over traditional vacuum tube transmitters for weather radar applications is lower life cycle cost due to higher reliability. However, because solid-state transmitters operate at lower voltages with smaller peak powers, they need to use longer pulses to reach the same level of target sensitivity as tube-based systems. An example is the Airport Surveillance Radar-11 (ASR-11) with a solid-state transmitter operating at 25-kW peak power and 9% duty cycle, which replaced the older ASR-8 with a Klystron transmitter operating at 1.4-MW peak power and 0.07% duty cycle. Although interference potential is linearly dependent on peak power, it increases nonlinearly with transmission duty cycle (Sanders et al. 2006). Therefore, all other parameters being equal, a radar with a solid-state transmitter will tend to have a higher potential for interfering with receivers compared to one with a tube-based transmitter.

Furthermore, communication devices, such as Wi-Fi transceivers, generally have duty cycles much higher than radars. These devices are rapidly proliferating around the world, and pulse interference filters are usually ineffective against this type of RFI. Thus, taken together with the growth of solid-state transmitters in radar systems, interference with weather radars—even those equipped with asynchronous pulse filters—can be expected only to worsen over time. It is desirable to develop RFI filtering mechanisms that are effective against higher duty cycle transmitters while avoiding false removal of weather signals.

2. Theoretical basis

Detecting RFI and discriminating it from weather signals can be framed in terms of base-band time series amplitude statistics. Since the I&Q base-band signal components at a given range gate are the result of summing over received signal from many scatterers that stochastically phase shift after each pulse period, the resulting distribution is Gaussian for both I and Q. The joint probability distribution of I and Q is the product of the individual probabilities, and the resulting I&Q time series amplitude distribution is a Rayleigh probability density function (e.g., Doviak and Zrnić 1993). The receiver noise distribution is independent of the weather signal distribution and is also Gaussian for I and Q. Since the sum of independent Gaussian processes results in a Gaussian distribution, the I&Q amplitude distribution for weather plus receiver noise is still Rayleigh distributed. The problem, then, is how to flag pulses within a processing dwell that appear to go above the bounds of a presumed Rayleigh amplitude distribution.

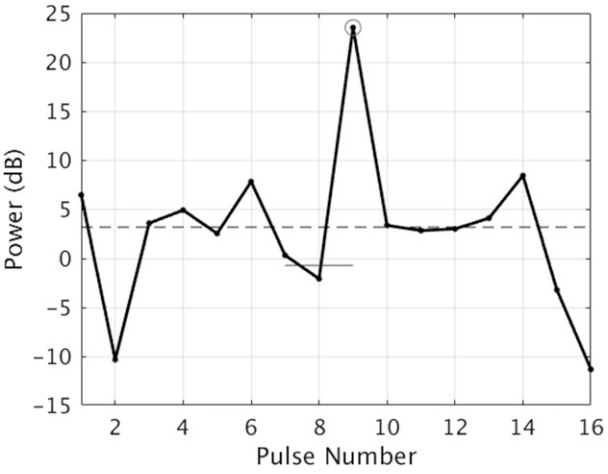

FIG. 1. Illustration for RFI detection in 1D. A CPI with 16 I&Q data points is shown with Rayleigh-distributed amplitudes except for an anomalously strong signal at pulse 9 (gray circle). Vertical scale is power in decibels. Shown are the median power over the CPI (dashed line), and the linearly averaged power over pulses 7 and 8 (solid gray horizontal line).

Current RFI detectors compare the amplitude (or power) of each pulse to that of its immediate neighbors or the median over the dwell (Vaisala 2016; Lake et al. 2014) [alternatively, a proposed method would use a chi-squared test to discriminate pulses that do not appear to fit into a Rayleigh amplitude distribution (Keränen et al. 2013)]. Figure 1 illustrates the first two mentioned methods. The median-based detection is simple—compute the median power over the coherent processing interval (CPI) and look for any points above a certain threshold over the median (dashed line in Fig. 1). Some data buffering is required to calculate the median. Note that the median is used instead of the mean, since it is less affected by spikes in power from sources such as RFI. A sliding window mean that excludes the pulse position

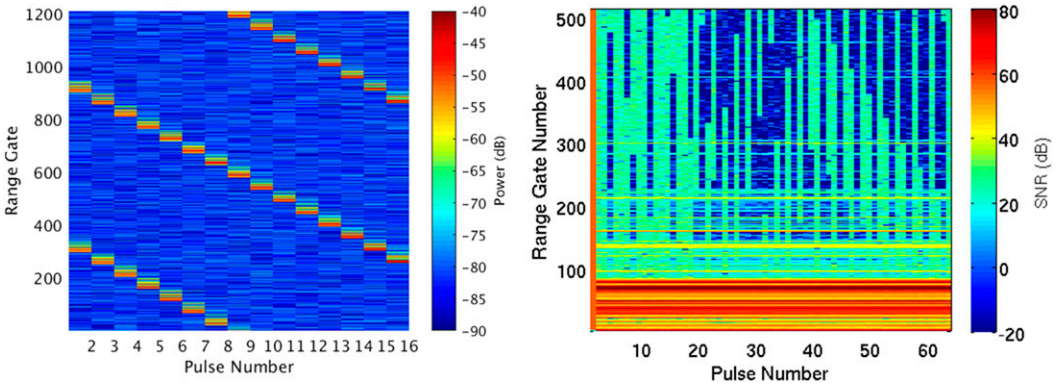

FIG. 2. RFI examples in 2D pulse number vs range gate domain. (left) Low duty cycle pulsed radar RFI received by the KMHX NEXRAD at 1845 UTC 25 Jun 2011. (right) High duty cycle Wi-Fi device RFI received by the PSF TDWR during an experiment at 1950 UTC 14 Dec 2010. Horizontal streaks are primarily ground clutter returns.

being evaluated, loosely analogous to a cell-averaging constant false alarm rate (CFAR) detector for aircraft detection (e.g., Barton 2005), might also be considered but that could still be contaminated by RFI in multiple pulses per dwell.

Vaisala's algorithm 3 (Vaisala-3) is currently used by the TDWR and looks only at three pulses at a time. For any pulse to be declared RFI, the absolute value of the difference in power between the previous two pulses must be below a certain threshold C_1, and the absolute value of the difference between the power and the linear average of the powers of the previous two pulses (solid gray horizontal line in Fig. 1) must exceed another threshold C_2. If any pulse power falls below the estimated receiver noise, then the noise power is used instead. Vaisala's three-point technique has the advantage of not assuming stationary statistics over the whole CPI, but its estimate of the background level using only two previous points is less robust. In either case, the computational burden is light and the performance is decent for RFI with high amplitude and low duty cycles. However, if the threshold for detection is set too low, then the false alarm rate becomes too high. Thus, the threshold must be kept high, which prevents weaker RFI from being flagged reliably. Also, as the interferer duty cycle rises, the chance that two or more consecutive pulses in the dwell get contaminated increases (Fig. 2). And in this case, the technique of comparing each pulse with its immediate neighbors does not work.

How does one improve the probability of detection P_D for weak RFI while suppressing the probability of false alarm P_{FA} as much as possible? Figure 2, right-hand panel, provides a clue. The problematic RFI cases (high duty cycles) generally have pulse lengths that are much longer than the range sampling interval of the receiving weather radar. This means that interference tends to exist along the "fast time" (range) dimension in multiple consecutive gates for a given pulse position in the "slow time" (pulse sample) dimension. Therefore, the extra information collected in the fast-time dimension can be used to improve the P_D and P_{FA} statistics. Specifically how this is done is explained below.

To illustrate with a concrete example, suppose that the I&Q weather signal amplitude distribution is given by

$$\frac{|V|}{\sigma^2} e^{-\frac{|V|^2}{2\sigma^2}}, \tag{1}$$

where $|V|$ is the signal amplitude and σ is the scale parameter of the Rayleigh distribution [and σ^2 is the mean-square value of I (equal to that of Q)]. The median of the distribution is $\sigma\,(2\ln 2)^{1/2}$, so we can define a ratio of signal power $|V|^2$ to the median power as

$$\Gamma = \frac{|V|^2}{2\sigma^2 \ln 2}. \tag{2}$$

The Rayleigh cumulative distribution function (CDF) for $|V|$ is $1 - e^{-|V|^2/(2\sigma^2)}$; rewriting it as a function of Γ using (2), we get $1 - e^{-\Gamma \ln 2}$. The probability that a given I&Q data point power exceeds the median signal power by factor Γ is 1 minus the CDF, which is $e^{-\Gamma \ln 2}$. Then the probability that the powers in the same I&Q data position in sample time across N consecutive range gates all exceed their respective median powers for each range gate—that is, P_{FA}—is $e^{-N\Gamma \ln 2}$. We choose the median rather than the mean as the baseline, because it is less susceptible to outliers (i.e., potential RFI signals) within the sample distribution. For a given P_{FA}, the RFI power detection threshold ratio is

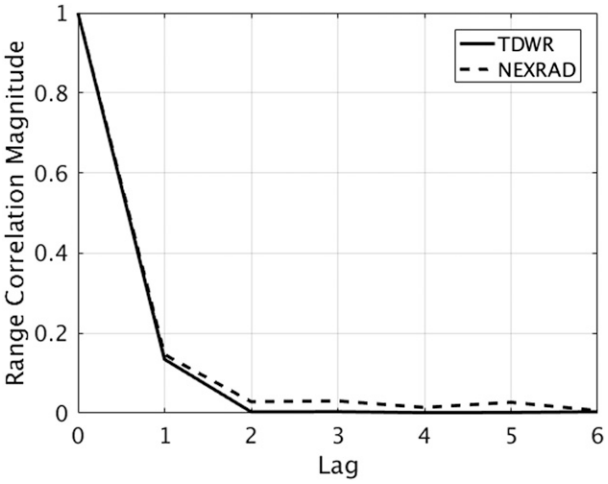

FIG. 3. Mean range correlation magnitude vs range lag computed for TDWR and NEXRAD I&Q data using (4) from Curtis and Torres (2013). Range and azimuth data were selected for fairly uniform weather without ground clutter or interference from the same data used for Fig. 10 (TDWR) and Fig. 12 (NEXRAD).

$$R = -\frac{\ln P_{\mathrm{FA}}}{N \ln 2}. \tag{3}$$

Thus, by examining N consecutive range gates instead of one, the same P_{FA} can be achieved with a lower R, which illustrates the advantage of expanding the RFI filter to two dimensions. In other words, RFI with lower interference-to-signal ratios (ISRs) or INRs can be detected without unduly increasing the P_{FA}. For example, if $P_{\mathrm{FA}} = 10^{-6}$ is desired, then the power ratio threshold (dB), $10 \log R$, can be reduced from 13 dB for $N = 1$ to 8.2 dB for $N = 3$. Note that the abovementioned discussion assumes that weather signals are uncorrelated in range time. This is a valid assumption for radars operating with range sample intervals matching the pulse width. (Figure 3 presents example mean range correlation magnitude versus range lag under fairly uniform weather conditions for TDWR and NEXRAD, showing rapid decorrelation with range as expected.) I&Q data that are oversampled in range violate this assumption.

In reality, however, it is impossible to estimate the median of the distribution with perfect accuracy, which degrades P_{FA} performance. In CFAR literature this is known as CFAR loss (Barton 2005). The estimate error depends on the number of data points available, that is, the number of pulses in a CPI [note that the median should not be taken over the entire two-dimensional (2D) domain, since each range gate can have different background weather signal powers]. Figure 4 shows the results of running Monte Carlo simulations of I&Q signal amplitudes with median powers estimated from CPIs with 16 and 64 data points. The difference between the simulation and theoretical result of (3) increases with fewer CPI pulses as expected.

The results of Fig. 4 would serve as an appropriate threshold lookup table for a 2D RFI detector if the interference amplitude over multiple range gates is constant. This is because the detection requirement of amplitude threshold exceedance over N consecutive gates is a good match to a steady interference signal. However, examination of wireless device signals received by TDWR shows that their amplitude variation over range gates is often noiselike (Cho 2011). A highly variable RFI signal will not reliably exceed detection thresholds over consecutive range gates. The solution is to base the detection condition on some sort of average across range gates. Consequently, we devised an alternative formulation of taking the mean of the power ratio (dB), MEAN($10 \log R$), over N consecutive range gates, as the threshold criterion. Ratios are calculated at each range gate, because the sample-time Rayleigh amplitude distributions are independent from gate to gate. The corresponding plots of averaged power ratios to P_{FA} are shown in Fig. 5. Comparing the results to Fig. 4, we can see that the price to be paid for robust detection of noisy interferers is a rise in detection thresholds for a given P_{FA}.

In both Figs. 4 and 5, the largest "gain" is obtained between $N = 1$ and $N = 3$—that is, just by including the pulse power statistics of the immediately adjacent range gates, the CFAR detection threshold can be lowered significantly. This is a useful result, because even low duty cycle pulsed radar RFI tends to span a few range gates for weather radars such as TDWR and NEXRAD with gate intervals of 150–250 m. An example of this can be seen in the left-hand panel of Fig. 2.

Table 1 summarizes the simulation results for use in the 2D filter algorithm that follows in the next section. The entries are RFI detection thresholds (dB) for power averaged over the given number of range gates and at the specified P_{FA}, as graphically shown in Fig. 5. The maximum range window length of 11 is arbitrary. This can certainly be extended to wider windows, and it will be effective on RFI cases that exist in consecutive range gates to those lengths. However, increased computational load will be a cost.

3. Algorithm for phased array radars

The discussion so far assumes that the I&Q amplitude distribution in each CPI and range gate is drawn from a statistically stationary pool. This is a good assumption with electronically scanned phased array radars with antenna beams that do not move during each CPI.

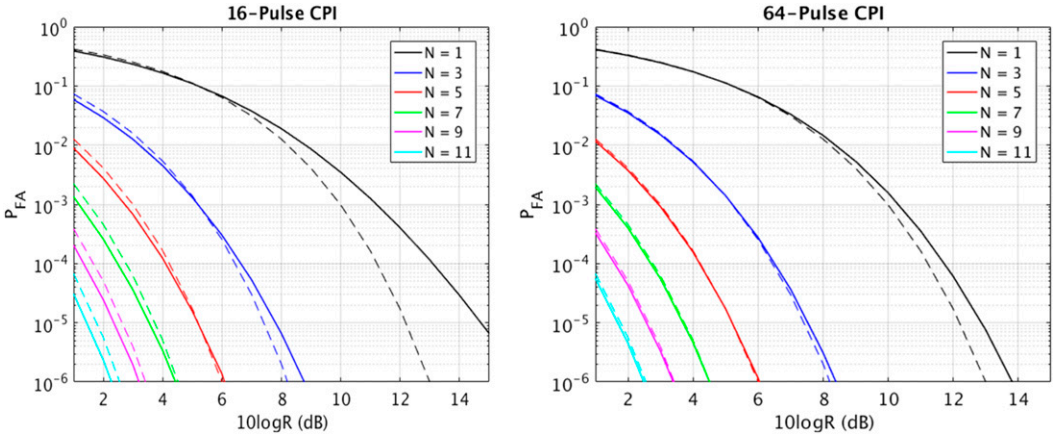

FIG. 4. Randomly generated Rayleigh-distributed numbers are used to compute the false alarm probabilities for the 2D RFI detector represented by (3). Number of pulses per CPI (over which the medians were computed) was (left) 16 and (right) 64. Shown are numerically calculated results (solid lines) and the theoretical limit (i.e., with perfectly accurate knowledge of the median values; dashed lines).

However, for radars with mechanically scanned dish antennas, the sampled volume changes with each pulse in the CPI; therefore, the samples may be polled from a distribution that is varying. This is a complication that is addressed in section 4. For now, we will describe the 2D RFI filter as implemented for an antenna beam that is stationary during each CPI.

The algorithm takes the excess-power-over-median approach and extends it to two dimensions. To illustrate, Fig. 6 shows simulated I&Q power over five range gates. The background amplitudes are Rayleigh distributed as from weather returns or noise. In pulse 9, additional power is injected to mimic RFI. Taking the middle panel (range gate 3), the power exceeds the median in the CPI by 7 dB. If we specify $P_{\mathrm{FA}} = 10^{-6}$, then we see from Table 1 that for a 16-pulse CPI and range gate window of length 1, the detection threshold is 16.3 dB. Thus, with the traditional one-dimensional approach, this would be a missed detection. However, if we extend the range gate window to length 3 and average the log-power ratio to the median over three gates, we get a mean excess of 12.7 dB, which exceeds the corresponding threshold of 10.1 dB. Similarly, a range gate window of length 5 yields an average power excess of 11.8 dB, which exceeds the corresponding 8.1-dB threshold.

The user can decide which range gate window lengths to incorporate into the RFI detector. For example, the window lengths 1 and 3 could be used in combination, or window lengths 1, 5, and 9. The trade-off is that as the number of window lengths used in combination is increased, the P_D will rise, but the cumulative P_{FA} and the computational burden will go up. For the rest of the paper, we will use lengths $N = 1, 3, 5, 7, 9$, and 11 with the windows centered on the gate of interest.

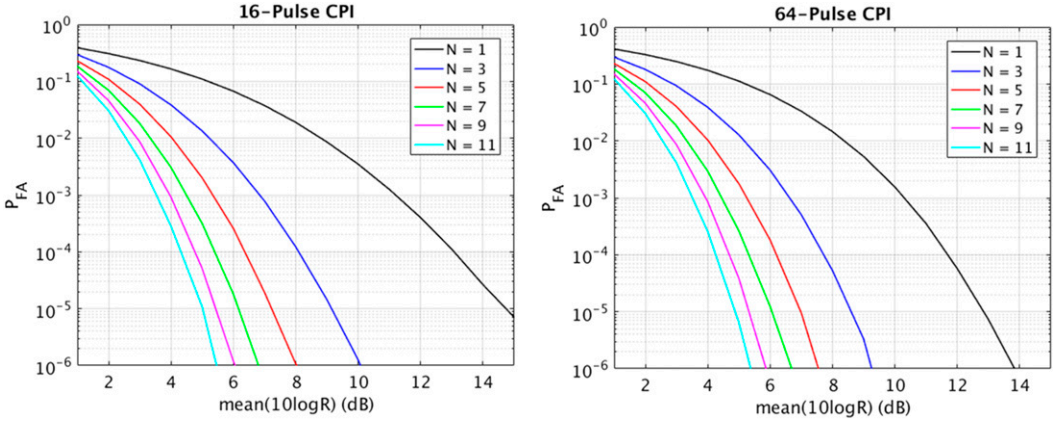

FIG. 5. Same as the numerically calculated results of Fig. 4, except that the power ratio threshold is averaged over N gates.

TABLE 1. 2D RFI detection thresholds (dB).

Range window length		1	3	5	7	9	11
8-pulse CPI	$P_{FA} = 10^{-6}$	18.8	10.8	8.3	7.0	6.3	5.5
	$P_{FA} = 10^{-5}$	17.0	9.6	7.5	6.3	5.5	5.0
	$P_{FA} = 10^{-4}$	14.7	8.4	6.5	5.4	4.8	4.3
16-pulse CPI	$P_{FA} = 10^{-6}$	16.3	10.1	8.1	6.7	6.0	5.4
	$P_{FA} = 10^{-5}$	14.8	9.1	7.3	6.2	5.4	5.1
	$P_{FA} = 10^{-4}$	13.1	8.1	6.3	5.4	4.8	4.3
32-pulse CPI	$P_{FA} = 10^{-6}$	14.8	9.5	7.7	6.6	5.9	5.4
	$P_{FA} = 10^{-5}$	13.5	8.8	7.1	6.1	5.4	5.0
	$P_{FA} = 10^{-4}$	12.2	7.8	6.2	5.4	4.8	4.3
64-pulse CPI	$P_{FA} = 10^{-6}$	13.8	9.2	7.5	6.6	5.9	5.3
	$P_{FA} = 10^{-5}$	12.9	8.6	7.0	6.1	5.4	4.9
	$P_{FA} = 10^{-4}$	11.7	7.7	6.2	5.4	4.8	4.3

The steps for the algorithm are shown below in Table 2.

Optimal data interpolation is not the subject of this paper. For the results shown in later sections, we employed linear interpolation across pulses for amplitude. The phase sequence in each CPI was unwrapped before linear interpolation was applied. Then the resulting phase information was added to the interpolated amplitudes with a complex exponential multiplication. [a simpler alternative is to linearly interpolate over the I (real) and Q (imaginary) series separately; however, doing this we found that the resulting amplitudes in the interpolated positions sometimes over- or undershot their neighbors, which was not good for display purposes]. If RFI detection flags were set at the edge of a CPI, we filled those positions with the same I&Q value of the nearest neighbor.

Also, for the lowest and highest range gate indices, the full range window span was not available. In those cases, the windows were truncated so that index i would not go below the first gate or above the last gate.

a. *Performance evaluation using simulated data*

The performance of the novel 2D RFI detector using simulated data is tested with the focus on Wi-Fi interference. To characterize the received signal amplitude statistics in I&Q data, we examined the data collected by the Federal Aviation Administration (FAA) Program Support Facility (PSF) TDWR during Wi-Fi RFI simulation on 17 June 2009. Three devices (Motorola Canopy, Cisco 802.11, and Axxcelera WiMax 802.16) were simulated using a vector signal generator, a device that can output a wide variety of industry-standard digitally modulated waveforms. Output power levels were systematically varied in the range −27 to +10 dBm. The signal was injected into a 40-dB reverse coupler in front of the waveguide switch (R. Gautam 2009, personal communication). The system noise power was about −109 dBm. For all three devices, the TDWR's signal power fits exponential distributions quite well (or, equivalently, Rayleigh distributions for the amplitudes). Figure 7 shows the histogram and best fit to an exponential for received I&Q power from simulated Motorola Canopy signals. Therefore, we will model Wi-Fi interference I&Q amplitudes using the noiselike Rayleigh distribution in the "fast" time dimension. (The amplitude statistics in the "slow" time domain will not be Rayleigh distributed, due to the irregular on/off transmission patterns.) This choice is conservative—if the Wi-Fi interference power in the I&Q data is steadier, then the 2D detector will perform even better than in the simulation. In general, Wi-Fi waveform characteristics vary depending on the device class, and the duty cycle will depend on the data throughput rate (Keränen et al. 2013).

To simulate a background of receiver noise (or weather), we used a matrix of 11 range gates × 64 pulses filled with randomly generated Rayleigh-distributed amplitudes. The scale parameter was arbitrarily set to one—the exact value does not matter, since the detection thresholds are independent of it [see, e.g., (3)]. However, by using the same scale parameter for all range gates, we are assuming that, for a weather background case, the weather SNR is constant over these gates. Additionally, we created an 11-gate vector filled with randomly generated Rayleigh-distributed amplitudes to represent the RFI signal present at a single pulse position (pulse 32). The RFI amplitudes were scaled so that the average power ratio to the noise, or the INR, was set to a specified value. Note that the INR could also be interpreted as the ISR, where "signal" means weather signal, since both weather returns and receiver noise have Rayleigh amplitude distributions. The RFI amplitudes were converted to complex values by multiplying with random-phase complex exponentials and then added to the noise amplitudes at pulse 32 (also converted to complex numbers using random phases). Absolute values of the complex sums were then taken to convert them back to amplitudes. The result was 11 consecutive range gates worth of 64-pulse CPIs of simulated I&Q amplitude data, where all gates at pulse 32 were contaminated by RFI with a specified mean INR.

The simulated data in the middle range gate (gate 6) was fed to the 1D RFI detectors, while the entire array was passed to the 2D RFI detector. For the Vaisala-3 algorithm, we set $C_1 = 11.8$ dB and $C_2 = 13.8$ dB. For the 1D median algorithm, we set the threshold to 13.8 dB. For the 2D RFI detector, we used the thresholds from the 64-pulse $P_{FA} = 10^{-6}$ entries in Table 1 (note that the

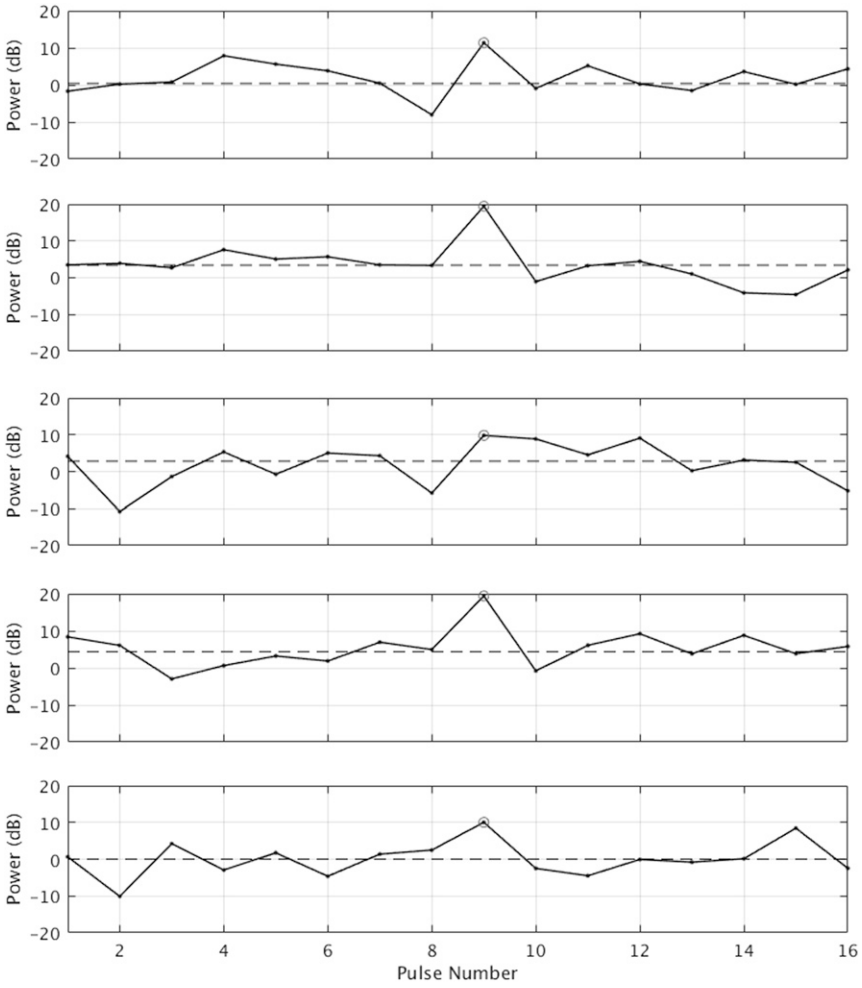

FIG. 6. Illustration for 2D RFI detection. Stacked plots show five consecutive range gates of Rayleigh-distributed I&Q amplitude [squared for power (dB)] over a 16-point dwell. Presence of added interference power is shown (gray circles).

single gate threshold for the 2D detector then is 13.8 dB, which aligns with the thresholds for the 1D cases). Three subcases were run for the 2D algorithm using two range windows (of lengths 1 and 3), four range windows (of lengths 1, 3, 5, and 7), and six range windows (of lengths 1, 3, 5, 7, 9, and 11).

Detection statistics were compiled based on the presence of RFI in gate 6, pulse 32. False alarm statistics were calculated based on all the other pulses in gate 6. Various INR values were tested, and 1 million Monte Carlo ''dice rolls'' per INR were conducted. The results are shown in Fig. 8. The 2D algorithm is clearly superior over all INRs, and the detection performance improves as the number of range gate windows used increases. This will be true as long as the interference persists in the range dimension inside the window spans. The P_{FA} values were 5×10^{-3} for Vaisala-3 and 1×10^{-6} for the 1D median algorithm (as expected, since the excess-over-median threshold was chosen based on $P_{\mathrm{FA}} = 10^{-6}$). For the 2D algorithm, the false alarms rates were 2×10^{-6} (two range windows), 4×10^{-6} (four range windows), and 6×10^{-6} (six range windows). The aggregate false alarm rates for the 2D detector increases linearly as more neighboring range gates are included as expected, a small price to pay for the nonlinear improvement in P_D at low INRs. There will, however, also be a cost in increased computational time as more range gate windows are included. This is a trade-off that should be studied in the future after the algorithm has been implemented in a real-time processing system.

As noted earlier, the simulation results shown in Fig. 8 assumed a constant Rayleigh scaling factor for all range gates, which is valid when the background is just system

TABLE 2. Steps for the algorithm.

1) Accumulate I&Q data over all range gates for a CPI in a 2D complex matrix with elements V_{ij}, where i is the range index and j is the pulse number.
2) Compute power, $p_{ij} = |V_{ij}|^2$, for all i and j.
3) Compute median power across the CPI M_i at each range.
4) Compute ratio of power to median (dB), $R_{ij}^{\mathrm{dB}} = 10\log(p_{ij}/M_i)$, for all i and j.
5) Initialize to false all members of a logical flag matrix with elements F_{ij}, matching the size of the R_{ij}^{dB} matrix.
6) For each pulse number j, do the following:
   (a) For each range gate i, do the following:
      (i) For each range window length N, do the following if F_{ij} is false:
         1) Compute the mean of R_{ij}^{dB} across the range window, i − FLOOR(N/2) to i + FLOOR(N/2), where "FLOOR" means rounding down to the nearest integer.
         2) If the mean of R_{ij}^{dB} is greater than the corresponding threshold from a lookup table such as Table 1, then set F_{ij} to true.
7) For each i, do the following:
   (a) If any F_{ij} is true, then fill the corresponding pulse position I&Q data with interpolated values.

noise or weather signal with no variability with range. Sharp gradients in weather reflectivity with range occur, of course. Thus, we introduced varying levels of background amplitude gradients in the simulation by using different Rayleigh scaling factors for different range gates. The results consistently showed, as in Fig. 8, the 2D algorithm significantly outperforming the 1D algorithms.

b. Demonstration on real data

In December 2010, three Wi-Fi devices were tested at the FAA PSF in Oklahoma City, Oklahoma. Each device was set up on a warehouse rooftop 4795 m from the PSF TDWR at 17.4° bearing with respect to magnetic north. The height of the rooftop was at 391 m MSL, which was 34 m below the altitude of the TDWR antenna feed horn. For each device type, an access point (master) and client devices were set up 1–8 m apart on the rooftop (Carroll et al. 2011).

Figure 9 shows TDWR I&Q data power in range versus pulse number format during a time when device C (an 802.11 Wi-Fi unit designed for indoor use) was transmitting. Its power output was set to maximum (17 dBm) with a bandwidth of 20 MHz and a center frequency matched to the TDWR's operating frequency (5620 MHz). The TDWR transmitted at a PRF of 1950 Hz, and its antenna was pointed directly at the device. Because the TDWR's antenna was not rotating, it is an appropriate stand-in for a phased array radar. The RFI filter algorithms discussed in the previous section with the same power thresholds were applied to the data. (For the 2D filter, six range windows of lengths 1, 3, 5, 7, 9, and 11 were used.) As with the simulations, the 2D filter significantly outperformed the other algorithms

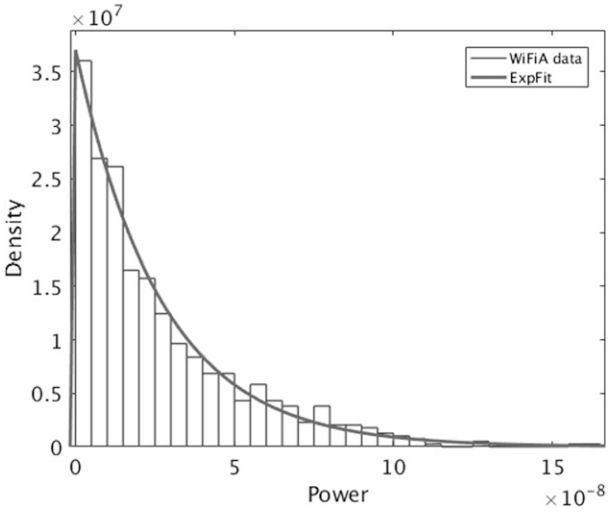

FIG. 7. Histogram and best fit to an exponential for I&Q power when simulated signals for a Motorola Canopy wireless transmitter was injected into the PSF TDWR receiver.

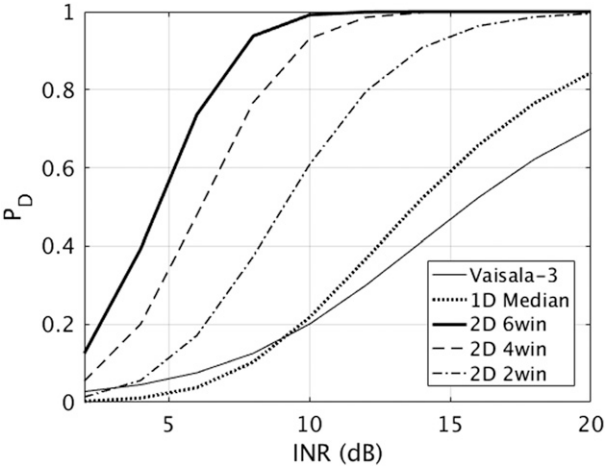

FIG. 8. RFI detection probability vs INR for the Vaisala-3, 1D median, and 2D algorithms. Monte Carlo simulation as described in the text was used to compute the results.

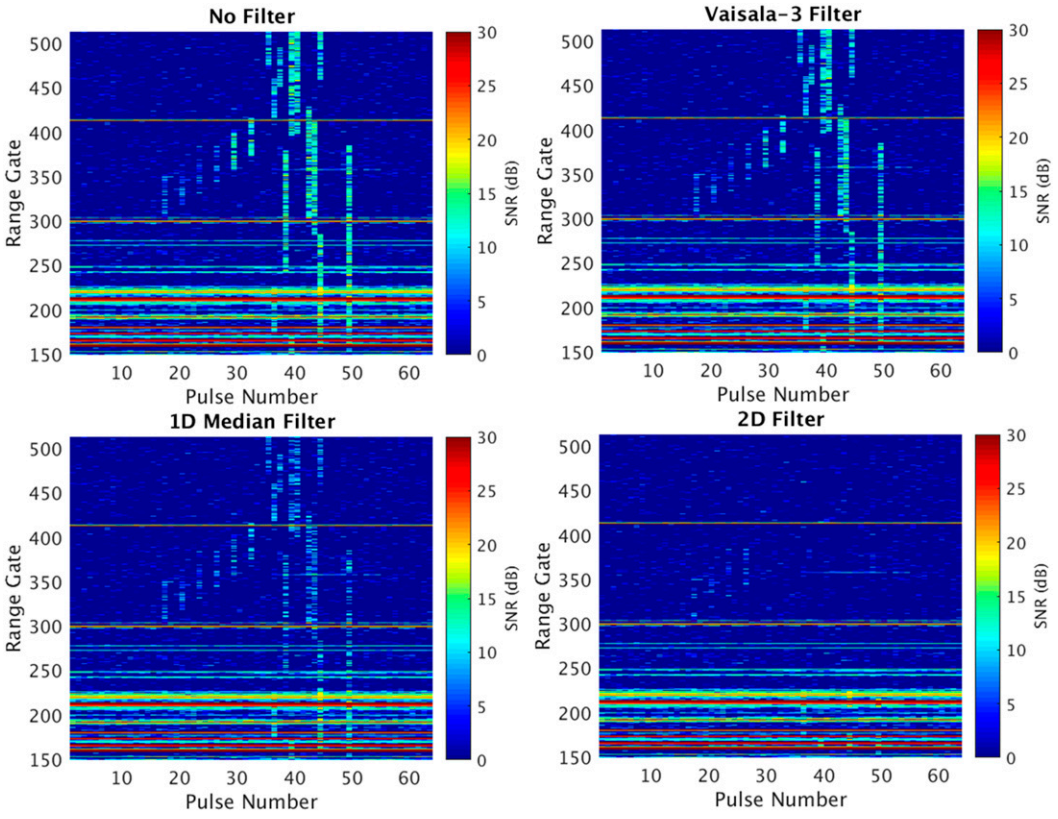

FIG. 9. Range vs pulse number plots of I&Q data SNR for (top left) no RFI filter, (top right) Vaisala-3 RFI filter, (bottom left) 1D median RFI filter, and (bottom right) 2D RFI filter. Data were collected at 1844 UTC 15 Dec 2010 by the PSF TDWR (Oklahoma City) with the antenna fixed at elevation angle 0.2° and azimuth angle 17.4°. An 802.11 Wi-Fi device was setup on top of a building 4.8 km from the radar within its line of sight. It transmitted at the center frequency of the TDWR. Clutter returns are shown (horizontal stripes)—it was a clear weather day.

in detection and filtering. Testing on other RFI datasets shows similar improvements. Note that the theoretical per-pulse false alarm rates are very low (6×10^{-6} for the 2D filter), so even better performance could be expected if higher false alarm rates could be tolerated.

4. Algorithm modification for mechanically rotating radars

As noted earlier, if the antenna beam is moved during a CPI, then the amplitude statistics of weather returns is no longer stationary. Also, ground clutter signal amplitudes can change dramatically as the antenna scans along each object. In this case, the median computed over a dwell may not be appropriate for all pulses in the dwell. If the whole-dwell median is always used on a mechanically scanned radar, then the false alarm rate for median-based RFI detection will be raised significantly over the theoretical values computed in section 2. The problem is illustrated in the left-hand panel of Fig. 10. The black circles denote the pulses that were declared to be interference by the 2D RFI detector. In this case all the data were either ground clutter (at near range) or weather (at far range), so the circles are false alarms. The clusters of false alarms on the ground clutter gates are especially problematic, since the replacement of all those consecutive pulses could have a detrimental effect on clutter filtering.

In principle, the most logical solution to the changing background amplitude statistics is to employ a sliding window median instead of a static whole-dwell median. For example, a window with the length of the CPI could be used to compute the median for every pulse position centered on the window within the dwell. This would necessitate buffering I&Q data over each dwell $\pm$½ CPI and recalculating the median for every pulse position. This is not unreasonable and likely implementable in most cases. However, as the 2D RFI filter already has an increased computational burden compared to the conventional 1D algorithms, a more efficient solution is desired for real-time implementation.

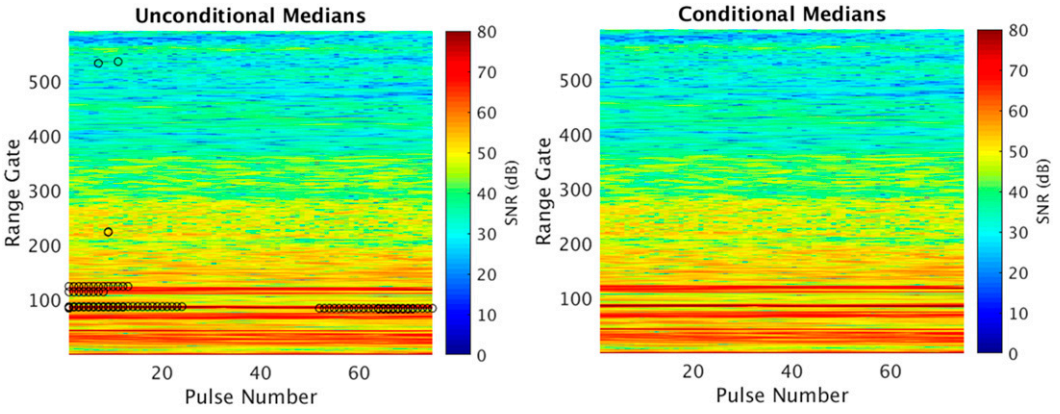

FIG. 10. Range vs pulse number plots of I&Q data SNR with 2D RFI filter applied with (left) whole-dwell median everywhere and (right) conditional medians as explained in the text. Pulses that were detected to be RFI and replaced (black circles). Data were collected by the PSF TDWR at 2321 UTC 5 Nov 2006 at elevation angle 0.3° and azimuth angle 17°, and a PRF of 1667 Hz.

We propose an alternative solution as follows. Between steps 3 and 4 in the 2D RFI filter algorithm described in Table 2, do the following: Divide each CPI into thirds and compute median powers over each third (left, center, right). If the ratio of a third-of-a-dwell median to the whole-dwell median is above a specified value, then the filter will use the partial-dwell median for pulses in the corresponding third of the CPI. As the purpose of using a more "local" median is to prevent unwanted false alarms from antenna rotation, that is, to be conservative, only positive deviations from the whole-dwell median are acted upon. Currently, we are using a linear factor of 2 for the partial-to-whole median threshold.

The result of applying this conditional median approach is shown in the right-hand panel of Fig. 10. There are no black circles, indicating that the false alarm rate has dropped to 0, which is the desired outcome. We also ran the simulation-based detection performance measurement from section 3a with the conditional median, and the results were indistinguishable from the run with the 2D detection algorithm with the unconditional median.

If this method of compensating for a nonstationary dwell is still yielding too many false alarms on ground clutter targets than is deemed acceptable, then an additional check could be put in place. The dominant presence of stationary ground clutter could be detected by computing the clutter phase alignment (CPA; Hubbert et al. 2009) over each dwell. If the CPA is greater than a threshold indicating high probability of clutter, then the RFI detection thresholds could be raised for that dwell, or the detector could be turned off altogether.

Further studies are needed to show what the false alarm rates are on a variety of weather and clutter conditions, to quantify the effects on base data quality, and ultimately to establish specifications for maximum acceptable false alarm rates.

Demonstration on real data

During Wi-Fi device testing at the FAA PSF in December 2010, data were collected by the TDWR in stationary pointing mode (e.g., Fig. 9) and in normal scanning modes. Signal from device A with its operating frequency set to match the TDWR's was detected in azimuths 13°–20° with the radar in monitor scanning mode for the lowest elevation angle of 0.3° (Cho 2011). (Device A is used by Internet service providers for fixed wireless networking.) The Wi-Fi signals were weak enough that even without any RFI filtering, visual evidence was visible only in the I&Q power plots and the spectrum width data. The device talk-to-listen ratio was fixed at 85:15, and its channel bandwidth was 20 MHz. So, this represented a very difficult case for RFI filtering of low INR and high duty cycle interferer. Figure 11 shows spectrum width plots of this case with and without the different RFI filters. The same threshold parameters applied in the previous section were used. Only the 2D RFI filter with its sensitivity to low INRs was able to significantly clean up the anomalously high spectrum widths in azimuths 13°–20°.

We can also compare the performance of the various filters on relatively high INR and low duty cycle RFI. The left-hand panel of Fig. 2 represents such a case. Even though the maximum INR per interfering pulse lands in only one or two range gates, the tails of the pulse extend across multiple gates at a much diminished power level. Thus, the 2D RFI filter can be more effective than the 1D counterparts even for this case. Figure 12 shows reflectivity plots from the KMHX NEXRAD in Morehead City, North Carolina, with

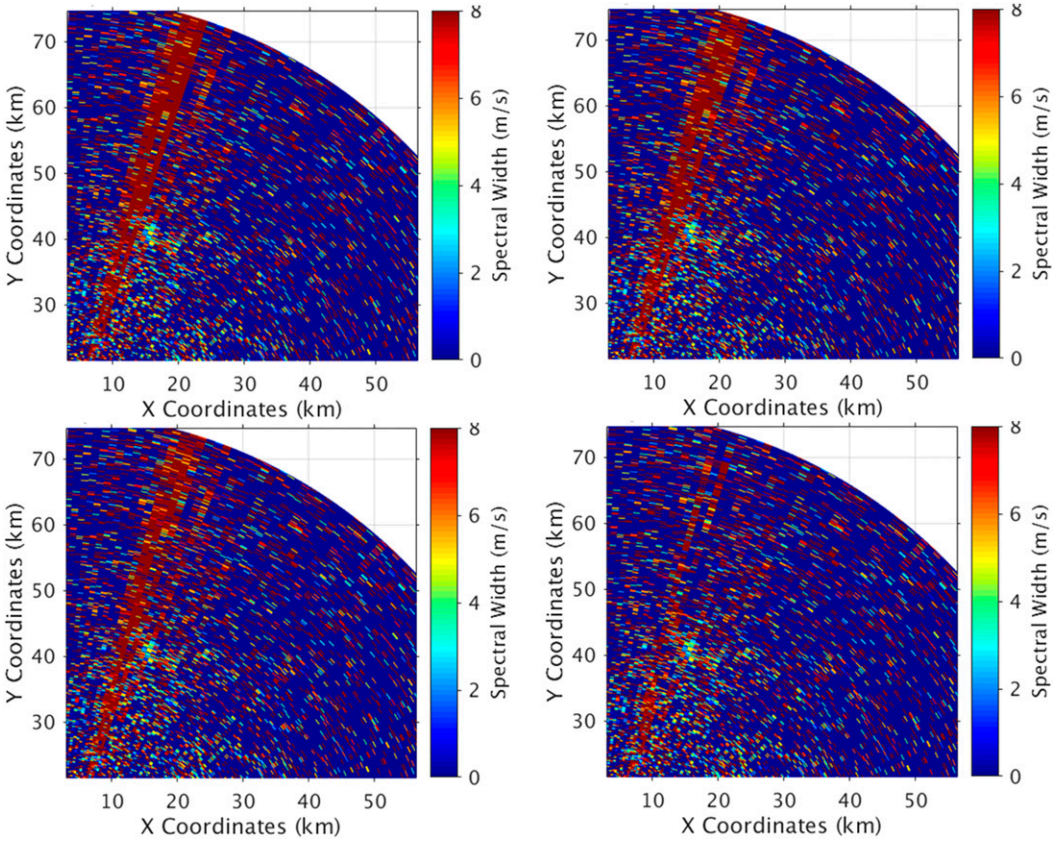

FIG. 11. Spectrum width (top left) with no RFI filter, (top right) with the Vaisala-3 filter, (bottom left) with the 1D median RFI filter, and (bottom right) with the 2D RFI filter. Data were collected with the PSF TDWR at elevation angle 0.2° at 2154 UTC 13 Dec 2010 with a PRF of 1930 Hz.

RFI-contaminated radials clearly visible to the west-southwest in the no-filter plot (top left). These are the same data from which Fig. 2 was drawn. More RFI signals are progressively filtered out with the application of the Vaisala-3 (top right), 1D median (bottom left), and 2D (bottom right) algorithms. Figure 13 shows spectrum width (the most sensitive base data field to RFI contamination) plots for the same data with similar results.

5. Other techniques

Amplitude anomaly detection is not the only way to flag and filter RFI. In the Doppler spectral domain, Wi-Fi interference in weather radars presents as white noise (Joe et al. 2005). Because this type of RFI appears as a raised spectrum noise floor and not a compact spectral feature, it is not possible to cleanly separate the interference spectrum from the weather spectrum. However, it is possible to detect the anomalous increase in the spectral noise floor and subtract the excess power. If the weather spectrum is not completely covered up by the rise in the noise floor, its moment estimates can be improved. In fact, such a procedure is used in the TDWR to extend the clutter suppression capability beyond the system stability limit (Cho 2010), and it was shown to be a viable technique for RFI suppression (Cho 2011) with the caveats mentioned above.

For weather radars with dual-polarization capability, a spectral polarimetric filter has been proposed (Rojas et al. 2012). As there is overlap in the spectral polarimetric properties of RFI and other signal types, the fuzzy classification algorithm cannot be expected to perform perfectly. However, Doppler spectral filtering is the only option when the duty cycle of the interferer surpasses ~50% (e.g., Fig. 2, right-hand panel), because in the time domain not enough clean data are left to provide a valid background distribution for detection and interpolation. In this sense time-domain and spectral-domain RFI filtering techniques are complementary, and they may be used together for maximum effectiveness to cover the entire interferer duty cycle space.

Finally, pulse phase information also has utility for RFI detection. Since weather signals have a phase

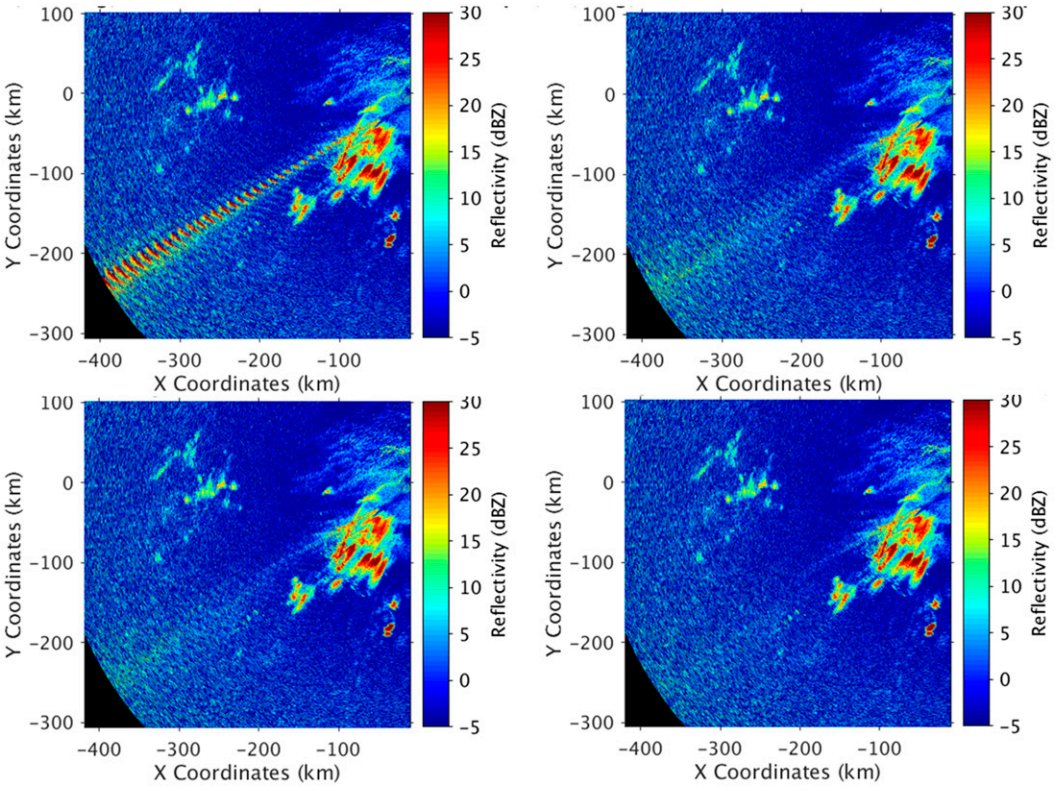

FIG. 12. Reflectivity (top left) with no RFI filter, (top right) with the Vaisala-3 filter, (bottom left) with the 1D median RFI filter, and (bottom right) with the 2D RFI filter. Data were collected with the KMHX NEXRAD on the lowest elevation angle and low-PRF mode during a volume coverage pattern (VCP) 21 scan at 1845 UTC 25 Jun 2011.

change trend from pulse to pulse (used to estimate the radial velocity), whereas RFI signals have random phase distribution across sample time, in principle this information can be used in addition to the amplitude data to discriminate between RFI and weather. Specifically, we were able to show that time-lag phase variance of weather and stationary ground clutter was noticeably different from that of RFI and receiver noise. Via a fuzzy logic combination with an amplitude exceedance interest field, we could improve the detection and false alarm rates over using the amplitude variable alone. However, the performance gain was small compared to extending the amplitude anomaly detection algorithm to 2D. Furthermore, the time-lag phase variance properties depended on weather signal spectrum width and SNR. In the end, therefore, we decided against incorporating this extra information into our amplitude-only 2D algorithm, especially since computational burden was a concern for real-time implementation.

6. Summary

We showed that amplitude-anomaly-based detection of RFI, when extended to the 2D range-and-sample-time domain, can be made more sensitive to low-INR (or low ISR) cases and more reliable for high-INR (or high ISR) cases. The 2D RFI filter is especially suitable for low to medium duty cycle interferers, such as Wi-Fi devices operating under moderate talk-to-listen ratios and radars. With the rising popularity of solid-state transmitters for radar, with duty cycles of ~10%, the 2D RFI filter could correspondingly grow to become an important tool for suppressing interference with weather radars.

The only drawback to this new algorithm is the increase in computational burden over the currently used 1D filters. However, its parameters can be adjusted to allow a direct trade-off between filtering performance and processor load. In the range-time dimension, the number of range gate windows used linearly impacts computational time. In the sample-time dimension, the whole-dwell median window could be split into subdivisions of the CPI (for stationary beams) or replaced by a very short moving median window (for continuously scanning beams) to reduce the computational load; there is a considerable history of research on fast sliding median calculations that could be leveraged (e.g., Juhola et al. 1991). This flexibility should allow the new

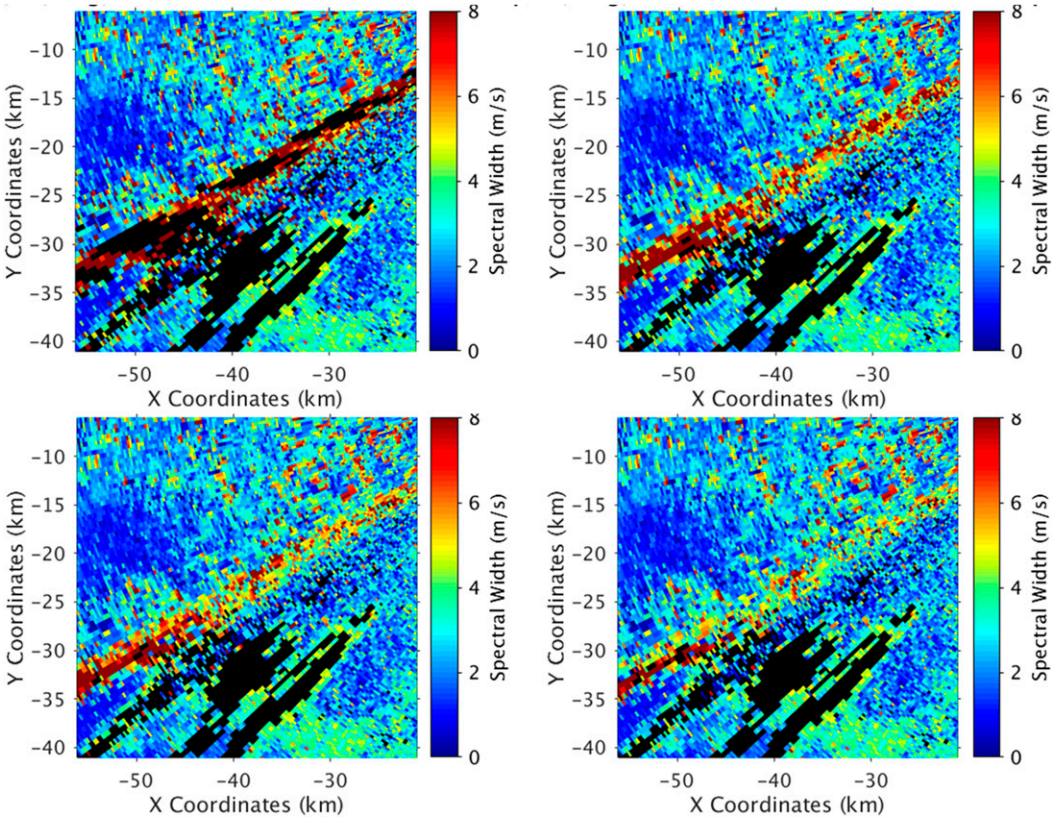

FIG. 13. Spectrum width (top left) with no RFI filter, (top right) with the Vaisala-3 filter, (bottom left) with the 1D median RFI filter, and (bottom right) with the 2D RFI filter. Data were collected with the KMHX NEXRAD on the lowest elevation angle and Doppler mode during a VCP 21 scan at 1846 UTC 25 Jun 2011. Black areas were censored by the ''invalid spectrum width'' flag.

2D algorithm to be implemented in most real-time signal processors in some form.

Finally, there is a new interagency program in the United States that is investigating the feasibility of opening up the 1.3–1.35-GHz RF window, currently reserved for federal systems, to auction for commercial bidders by 2024. Dubbed the Spectrum Efficient National Surveillance Radar (SENSR) program, it brings together the FAA, the National Oceanic and Atmospheric Administration, the Department of Defense, and the Department of Homeland Security for coordinated planning of the future national airspace surveillance infrastructure (e.g., Rockwell 2017). Clearly, optimizing radar network spectrum usage is a primary concern for SENSR, and improved tolerance for interference through means, such as the 2D RFI filter, is a key objective.

One potential solution for SENSR is consolidating some or all of the legacy radar functions into a single type of multifunction phased array radar (MPAR; Weber et al. 2007). As noted earlier, phased arrays with their stationary antenna positions over each CPI fit particularly well with the 2D RFI filter algorithm. We suggest that further testing of this new algorithm be conducted with MPAR proof-of-concept systems such as the Advanced Technology Demonstrator (Stailey and Hondl 2016).

Acknowledgments. This material is based upon work supported under U.S. Air Force Contract FA8702-15-D-0001. Any opinions, findings, conclusions, or recommendations expressed in this material are those of the author and do not necessarily reflect the views of the U.S. Air Force. I thank Jennifer Atkinson, NEXRAD FAA liaison, for noting the KMHX interference case and making the I&Q data available to us. I also acknowledge Steve Kim, the FAA Aviation Weather Sensors program manager, for supporting this work.

REFERENCES

Barton, D. K., 2005: *Radar System Analysis and Modeling.* Artech House, 545 pp.

Carroll, J. E., G. A. Sanders, F. H. Sanders, and R. L. Sole, 2011: Case study: Investigation of interference into 5 GHz weather

radars from unlicensed national information infrastructure devices, Part II. Department of Commerce NTIA Rep. TR-11-479, 28 pp. [Available online at https://www.its.bldrdoc.gov/publications/download/11-479.pdf.]

Cho, J. Y. N., 2010: Signal processing algorithms for the Terminal Doppler Weather Radar: Build 2. MIT Lincoln Laboratory Project Rep. ATC-363, 79 pp. [Available online at http://www.ll.mit.edu/mission/aviation/publications/publication-files/atc-reports/Cho_2010_ATC-363_WW-20740.pdf.]

——, 2011: Analysis of 5-GHz U-NII device signals received by the PSF TDWR. MIT Lincoln Laboratory Project Memo. 43PM-Wx-0119, 28 pp.

Curtis, C. D., and S. M. Torres, 2013: Real-time measurement of the range correlation for range oversampling processing. *J. Atmos. Oceanic Technol.*, **30**, 2885–2895, doi:10.1175/JTECH-D-13-00090.1.

Doviak, R. J., and D. S. Zrnić, 1993: *Doppler Radar and Weather Observations.* Academic Press, 562 pp.

FAA, 1995: Specification: Terminal Doppler Weather Radar with enhancements. Federal Aviation Administration Doc. FAA-E-2806c, 142 pp.

Hubbert, J. C., M. Dixon, S. M. Ellis, and G. Meymaris, 2009: Weather radar ground clutter. Part I: Identification, modeling, and simulation. *J. Atmos. Oceanic Technol.*, **26**, 1165–1180, doi:10.1175/2009JTECHA1159.1.

Joe, P., J. Scott, J. Sydor, A. Brandão, and A. Yongacoglu, 2005: Radio Local Area Network (RLAN) and C-band weather radar interference studies. *32nd Radar Conf. on Radar Meteorology*, Albuquerque, NM, Amer. Meteor. Soc., 8R.6. [Available online at https://ams.confex.com/ams/32Rad11Meso/techprogram/paper_97361.htm.]

Juhola, M., J. Katajainen, and T. Raita, 1991: Comparison of algorithms for standard median filtering. *IEEE Trans. Signal Process.*, **39**, 204–208, doi:10.1109/78.80784.

Keränen, R., L. Rojas, and P. Nyberg, 2013: Progress in mitigation of WLAN interferences at weather radar. *36th Conf. on Radar Meteorology*, Breckenridge, CO, Amer. Meteor. Soc., 336. [Available online at https://ams.confex.com/ams/36Radar/webprogram/Manuscript/Paper229098/AMS_36th_Radar_P15P336_Mitigation_WLAN_Interferences.pdf.]

Lake, J. L., M. Yeary, and C. D. Curtis, 2014: Adaptive radio frequency interference mitigation techniques at the National Weather Radar Testbed: First results. *Proc. 2014 IEEE Radar Conf.*, Cincinnati, OH, IEEE, 840–845, doi:10.1109/RADAR.2014.6875707.

NTIA, 2015: Manual of regulations and procedures for federal radio frequency management. National Telecommunications and Information Administration, 802 pp. [Available online at https://www.ntia.doc.gov/files/ntia/publications/manual_sep_2015.pdf.]

Obama, B., 2010: Unleashing the wireless broadband revolution. Presidential Memorandum for the Heads of Executive Departments and Agencies, Office of the Press Secretary, White House, 7 pp. [Available online at http://www.gpo.gov/fdsys/pkg/CFR-2011-title3-vol1/pdf/CFR-2011-title3-vol1-other-id236.pdf.]

Rockwell, M., 2017: FAA looks to spur spectrum sharing tech. [Available online at https://fcw.com/articles/2017/01/06/faa-spectrum-sensr.aspx.]

Rojas, L., D. N. Moisseev, V. Chandrasekar, J. Selzler, and R. Keränen, 2012: Dual-polarization spectral filter for radio frequency interference suppression. Preprints, *Seventh European Conf. on Radar in Meteorology and Hydrology (ERAD 2012)*, Toulouse, France, Météo-France, 194-SP. [Available online at http://www.meteo.fr/cic/meetings/2012/ERAD/extended_abs/SP_326_ext_abs.pdf.]

Saltikoff, E., J. Y. N. Cho, P. Tristant, A. Huuskonen, L. Allmon, R. Cook, E. Becker, and P. Joe, 2016: The threat to weather radars by wireless technology. *Bull. Amer. Meteor. Soc.*, **97**, 1159–1167, doi:10.1175/BAMS-D-15-00048.1.

Sanders, F. H., R. L. Sole, B. L. Bedford, D. Franc, and T. Pawlowitz, 2006: Effects of RF interference on radar receivers. Department of Commerce NTIA Rep. TR-06-444, 162 pp. [Available online at https://www.its.bldrdoc.gov/publications/download/TR-06-444.pdf.]

Stailey, J. E., and K. D. Hondl, 2016: Multifunction phased array radar for aircraft and weather surveillance. *Proc. IEEE*, **104**, 649–659, doi:10.1109/JPROC.2015.2491179.

Vaisala, 2016: User's manual: RVP900 digital receiver and signal processor. Vaisala Oyj, 513 pp. [Available online at ftp://ftp.sigmet.com/outgoing/manuals/RVP900_Users_Manual.pdf.]

Weber, M. E., J. Y. N. Cho, J. S. Herd, J. M. Flavin, W. E. Benner, and G. S. Torok, 2007: The next-generation multimission U.S. surveillance radar network. *Bull. Amer. Meteor. Soc.*, **88**, 1739–1751, doi:10.1175/BAMS-88-11-1739.